Quantum noise in optical fibers. II. Raman jitter in soliton communications

J. F. Corney

Department of Physics, The University of Queensland, St. Lucia, QLD 4072, Australia, and Department of Mathematical Modelling, Technical University of Denmark, DK-2800 Lyngby, Denmark

P. D. Drummond

Department of Physics, The University of Queensland, St. Lucia, QLD 4072, Australia

The dynamics of a soliton propagating in a single-mode optical fiber with gain, loss, and Raman coupling to thermal phonons is analyzed. Using both soliton perturbation theory and exact numerical techniques, we propose that intrinsic thermal quantum noise from the phonon reservoirs is a larger source of jitter and other perturbations than the gain-related Gordon–Haus noise for short pulses (≤ 1 ps), assuming typical fiber parameters. The size of the Raman timing jitter is evaluated for both bright and dark (topological) solitons and is larger for bright solitons. Because Raman thermal quantum noise is a nonlinear, multiplicative noise source, these effects are stronger for the more intense pulses that are needed to propagate as solitons in the short-pulse regime. Thus Raman noise may place additional limitations on fiber-optical communications and networking by use of ultrafast (subpicosecond) pulses. © 2001 Optical Society of America

OCIS codes: 060.4510, 270.5530, 270.3430, 190.4370, 190.5650, 060.2400.

1. INTRODUCTION

In this paper we analyze in some detail the effects of Raman noise on solitons. In particular, we derive approximate analytic expressions and provide further details of the precise numerical results published earlier.[1] The motivation for this study is essentially the finding that coupling to phonons is one property of a solid medium that definitely does not obey the nonlinear Schrödinger (NLS) equation. The presence of Raman interactions plays a major role in perturbing the fundamental soliton behavior of the NLS equation in optical fibers. This perturbation is in addition to the more straightforward gain and loss effects that produce the well-known Gordon–Haus effect.[2]

The complete derivation of the quantum theory for optical fibers was given in an earlier paper,[3] denoted QNI. In QNI a detailed derivation of the quantum Hamiltonian was presented that included quantum-noise effects owing to nonlinearities, gain, loss, Raman reservoirs, and Brillouin scattering. Phase-space techniques allowed the quantum Heisenberg equations of motion to be mapped onto stochastic partial differential equations. The result was a generalized NLS equation that can be solved numerically or with perturbative analytical techniques.

The starting point for this paper is the phase-space equation for the case of a single polarization mode, obtained with a truncated Wigner representation, which is accurate in the limit of large photon number. We use both soliton perturbation theory and numerical integration of the phase-space equation to calculate effects on soliton propagation of all known quantum-noise sources, with good agreement between the two methods.

Our main result is that the Raman noise that is due to thermal phonon reservoirs is strongly dependent on both temperature and pulse intensity. This means that at room temperature, Raman jitter and phase noise become steadily more important as the pulse intensity is increased, which occurs when a shorter soliton pulse is required for a given fiber dispersion. Using typical fiber parameters, we estimate that Raman-induced jitter is more important than the well-known Gordon–Haus jitter for pulses shorter than approximately 1 ps. Although we do not analyze them in detail here, we note that similar perturbations may occur during the collision of short pulses in a frequency-multiplexed environment.

2. RAMAN–SCHRÖDINGER MODEL

We begin with the Raman-modified stochastic NLS equation [Eq. (6.3) of QNI], obtained with the Wigner representation, for simplicity:

$$
\frac{\partial}{\partial \zeta} \phi(\tau, \zeta) = - \int_0^\infty \mathrm{d}\tau' g(\tau - \tau') \phi(\tau', \zeta) + \Gamma(\tau, \zeta)
$$

$$
+ i \left[\pm \frac{1}{2} \frac{\partial^2 \phi}{\partial \tau^2} + \int_0^\infty \mathrm{d}\tau' h(\tau - \tau') [\phi(\tau', \zeta)]^* \right.
$$

$$
\left. \times \phi(\tau', \zeta) + i \Gamma^R(\tau, \zeta) \right] \phi(\tau, \zeta). \tag{2.1}
$$

Here $\phi = \Psi \sqrt{v t_0 / \bar{n}}$ is a dimensionless photon field amplitude and $\tau = (t - x/v)/t_0$ and $\zeta = x/x_0$, where t_0 is a typical pulse duration used for scaling purposes and $x_0 = t_0^2/|k''|$ is a characteristic dispersion length. Group velocity v and dispersion relation k'' are calculated at carrier frequency ω_0.

Apart from a cutoff-dependent vacuum noise, the photon flux is $\mathcal{J} = |\phi|^2 \bar{n}/t_0$, where $\bar{n} = |k''|\mathcal{A}c/(n_2\hbar\omega_0^2 t_0)$ $= v^2 t_0/\chi x_0$ is the typical number of photons in a soliton pulse of width t_0, again for scaling purposes. In this definition, the fiber is assumed to have a modal cross-sectional area $\mathcal{A}$ and a change in refractive index per unit intensity of n_2. The positive sign in front of the second derivative term applies for anomalous dispersion ($k'' < 0$), and the negative sign applies for normal dispersion ($k'' > 0$). The functions g and h are gain–loss and Raman scattering response functions, respectively, and Γ and Γ^R are stochastic terms, discussed below.

Similar, but more accurate, equations occur with the positive-P representation, although in this case the phase-space dimension is doubled. To simplify the calculations further, we assume that gain and loss in the fiber are broadband relative to the soliton bandwidth and balance exactly. This requires that the amplifier sections in the fiber be sufficiently close together (of the order of the soliton scaling length or less) that the soliton can propagate without distortion.[4]

For the analytic calculations we also assume that the Raman nonlinear response function is instantaneous on the time scale of the soliton width. This is equivalent to assuming that the phonon modes are heavily damped and means that the Raman coupling leads only to incoherent scattering of the propagating radiation. Although this approximation neglects the well-known self-frequency shift,[5-7] we find that the self-frequency shift by itself is not a major cause of jitter for the distance scales that we consider here. This assumption can be improved at the expense of more-complicated analytic calculations. However, the full equations are used in the numerical simulations, which agree quite well with our analytical predictions.

The Raman-modified equation then reduces to

$$\frac{\partial}{\partial\zeta}\phi(\tau,\zeta) = \left[\pm\frac{i}{2}\frac{\partial^2}{\partial\tau^2} + i\phi^*(\tau,\zeta)\phi(\tau,\zeta)\right]$$
$$\times \phi(\tau,\zeta) + \Gamma^C(\tau,\zeta), \qquad (2.2)$$

where the term in brackets represents the usual NLS equation in normalized, propagative form. The combined noise sources have been grouped together as

$$\Gamma^C(\tau,\zeta) = \Gamma(\tau,\zeta) + i\Gamma^R(\tau,\zeta)\phi(\tau,\zeta). \qquad (2.3)$$

A. Initial Conditions and Quantum Evolution

Equation (2.2) is a complex-number equation that can accurately represent quantum-operator evolution through the inclusion of various noise sources. In the absence of any noise sources, Eq. (2.2) reduces to the classical NLS equation. This deterministic limit corresponds to taking $\bar{n} \to \infty$. As well as the noise sources that explicitly appear in Eq. (2.2), there must be noise in the initial conditions to properly represent a quantum state in the Wigner representation. Regardless of the initial quantum state chosen, there must be at least a minimal level of initial fluctuations in ϕ to satisfy Heisenberg's uncertainty principle. We choose to begin with a multimode coherent state, which contains this minimal level of initial quantum noise and which is an accurate model of mode-locked

laser output. This is also the simplest model for the output of mode-locked lasers, and we note that, in general, there could be extra technical noise. For coherent inputs, the Wigner vacuum fluctuations are Gaussian and are correlated as

$$\langle\Delta\phi(\tau,0)\Delta\phi^*(\tau',0)\rangle = \frac{1}{2\bar{n}}\delta(\tau - \tau'). \qquad (2.4)$$

Physical quantities can be calculated from this phase-space simulation by averaging of the products of ϕ and ϕ^* over many stochastic trajectories. In this Wigner representation these stochastic averages correspond to the ensemble averages of symmetrically ordered products of quantum operators, such as those that represent homodyne measurements and other measurements of phase.

B. Wigner Noise

Both fiber loss and the presence of a gain medium contribute quantum noise to the equations in the symmetrically ordered Wigner representation. The complex gain–absorption noise enters the NLS equation through an additive stochastic term Γ, whose correlations are

$$\langle\Gamma(\Omega,\zeta)\Gamma^*(\Omega',\zeta')\rangle = \frac{(\alpha^G + \alpha^A)}{2\bar{n}}\delta(\zeta - \zeta')\delta(\Omega + \Omega'), \qquad (2.5)$$

where $\Gamma(\Omega,\zeta)$ is the Fourier transform of the noise source:

$$\Gamma(\Omega,\zeta) = \frac{1}{\sqrt{2\pi}}\int_{-\infty}^{\infty}d\tau\Gamma(\tau,\zeta)\exp(i\Omega\tau). \qquad (2.6)$$

The dimensionless intensity gain and loss are given by α^G and α^A, respectively.

Similarly, the real Raman noise, which appears as a multiplicative stochastic variable Γ^R, has correlations

$$\langle\Gamma^R(\Omega,\zeta)\Gamma^R(\Omega',\zeta')\rangle = \frac{1}{\bar{n}}\delta(\zeta - \zeta')\delta(\Omega + \Omega')$$
$$\times \left[n_{\text{th}}(\Omega) + \frac{1}{2}\right]\alpha^R(\Omega), \qquad (2.7)$$

where the thermal Bose distribution is given by $n_{\text{th}}(\Omega)$ $= [\exp(\hbar|\Omega|/k_B T t_0) - 1]^{-1}$ and where $\alpha^R(\Omega)$ is the Raman gain, whose profile is given in Fig. 1 of QNI. Thus the Raman noise is strongly temperature dependent, but it also contains a spontaneous component that provides vacuum fluctuations even at $T = 0$.

As the $\bar{n}$ dependence of all the noise correlations shows, the classical limit of these quantum calculations is the deterministic NLS equation. The problem of jitter in soliton communications is an example of ways in which intrinsic quantum features can have a direct macroscopic consequence, even in a way that impinges on current developments of applied technology. There are, of course, classical contributions to jitter, such as noise that arises from technical sources. However, it is the jitter contributions from essentially quantum processes, namely, spontaneous emission in fiber amplifiers, that are the current limiting factor in soliton-based communications systems. Other jitter calculations rely on a classical formulation

with an empirical addition of amplifier noise, and important predictions of the Gordon–Haus effect have been obtained. Nevertheless, the quantum treatment presented here of all known noise sources is necessary for determining the limiting effects of other intrinsic noise sources, which become important for shorter pulses and longer dispersion lengths.

In the absence of the noise sources, the phase-space equations have stationary solutions in the form of bright (+) or dark (−) solitons. Solitons are solitary waves in which the effects of dispersion are balanced by nonlinear effects to produce a stationary pulse that is robust in the presence of perturbations. We note here that, in reality, the Raman response function is noninstantaneous, which causes a redshift in the soliton frequency. This soliton self-frequency shift is a deterministic effect and so can be neglected in the treatment of noise effects to a first approximation. The accuracy of this approximation will be evident in the subsequent comparison of analytic with numerical results. The numerical results all include the complete nonlinear response function rather than the approximate instantaneous form given above.

Excessive self-frequency shift may cause problems when finite bandwidth elements are used. However, it has been shown[8] that bandwidth-limited gain can in fact cancel the effect of the Raman redshift by pulling the soliton back toward the center of the spectral band. In the simulations that we show in this paper, the total redshift is estimated to be $\Delta f \simeq 0.02\,\mathrm{THz}$, which is small compared with the total width of the gain spectrum in typical fiber laser amplifiers ($\Delta \nu \simeq 3\,\mathrm{THz}$).[9]

3. PERTURBATION THEORY

We now proceed to derive the approximate analytic expressions for the effects of noise on soliton jitter, using soliton perturbation theory,[10–15] for both bright and dark solitons.

A. Bright Solitons
The stationary soliton of Eq. (2.2) for anomalous dispersion is

$$\phi_{\mathrm{bright}}(\tau, \zeta) = A \operatorname{sech}[A\tau - q(\zeta)]\exp[iV\tau + i\theta(\zeta)],$$

(3.1)

where $\partial q/\partial \zeta = VA$ and $\partial \theta/\partial \zeta = (A^2 - V^2)/2$, with amplitude A and velocity V. Following the method presented by Haus $et\ al.$,[11,12] we treat the effects of the noise terms as perturbations about a soliton solution whose parameters vary slowly with ζ:

$$\phi(\tau, \zeta) = \bar{\phi}(\tau, \zeta) + \Delta\phi(\tau, \zeta),$$

(3.2)

where the unperturbed-soliton solution is given by

$$\bar{\phi}(\tau, \zeta) = A(\zeta)\operatorname{sech}[A(\zeta)\tau - q\zeta]\exp[iV(\zeta)\tau + i\theta(\zeta)]$$

(3.3)

for a bright soliton. Substituting Eq. (3.2) into Eq. (2.2)

gives the following linearized equation [first order in $\Delta\phi(\tau, \zeta)$]:

$$\frac{\partial}{\partial \zeta}\Delta\phi(\tau, \zeta) = \left[\pm\frac{i}{2}\frac{\partial^2}{\partial \tau^2} + i2\bar{\phi}^*(\tau, \zeta)\,\bar{\phi}(\tau, \zeta)\right]$$
$$\times \Delta\phi(\tau,\zeta) + i\bar{\phi}(\tau, \zeta)^2\Delta\phi^*(\tau, \zeta) + \bar{\Gamma}(\tau, \zeta),$$

(3.4)

where the linearized noise source $\bar{\Gamma}(\tau, \zeta)$ is defined as

$$\bar{\Gamma}(\tau, \zeta) = \Gamma(\tau, \zeta) + i\Gamma^R(\tau, \zeta)\bar{\phi}(\tau, \zeta).$$

(3.5)

Now we wish to determine the evolution of the soliton parameters as a function of propagation distance ζ. To do this, we expand the perturbation in terms of the soliton parameters plus a continuum term:

$$\Delta\phi(\tau, \zeta) = \sum_i \frac{\partial\bar{\phi}(\tau, \zeta)}{\partial P_i}\Delta P_i + \Delta\phi_c(\tau, \zeta)$$

$$= \sum_i f_{P_i}\Delta P_i + \Delta\phi_c(\tau, \zeta),$$

(3.6)

where $P_i \in \{V, q, A, \theta\}$. The projection functions for these parameters are

$$f_A = [(1/A) - \tau\tanh(A\tau - q)]\bar{\phi},$$
$$f_q = \tanh(A\tau - q)\bar{\phi},$$
$$f_V = i\tau\bar{\phi},$$
$$f_\theta = i\bar{\phi}.$$

(3.7)

Inasmuch as linearized equation (3.4) is not self-adjoint, these eigenfunctions are not orthogonal. To select out the evolution of particular parameters, we therefore choose an alternative set of functions:

$$\overline{f_A} = \bar{\phi},$$
$$\overline{f_q} = \tau\bar{\phi},$$
$$\overline{f_V} = i\tanh(A\tau - q)\bar{\phi},$$
$$\overline{f_\theta} = i\tau\tanh(A\tau - q)\bar{\phi}.$$

(3.8)

These are the eigenfunctions of the adjoint equation to Eq. (3.4) and obey the orthogonality condition

$$\Re\left(\int_{-\infty}^{\infty} d\tau f_{P_i}\overline{f_{P_j}}^*\right) = \delta_{i,j}.$$

(3.9)

Substituting the Taylor expansion [Eq. (3.6)] into the linearized equation [Eq. (3.4)] and using the functions $\overline{f_{P_i}}$ to project out particular parameters show that the growth of fluctuations in position Δq is governed by

$$\frac{\partial}{\partial \zeta}\Delta q(\zeta) = A\Delta V(\zeta) + \Gamma_q(\zeta),$$

$$\frac{\partial}{\partial \zeta}\Delta V(\zeta) = \Gamma_V(\zeta),$$

(3.10)

where we have taken the unperturbed velocity to be zero: $V = 0$. The stochastic terms are defined as

$$\Gamma_{P_i}(\zeta) = \Re\left[\int_{-\infty}^{\infty} d\tau \overline{f_p}^*(\zeta)\overline{\Gamma}(\tau, \zeta) \right]. \qquad (3.11)$$

Here we have assumed that the perturbations in the continuum ϕ_c are orthogonal to $\overline{f}_{P_i}$, a condition that depends on such perturbations' dispersing sufficiently rapidly away from the region about the soliton. In fact, any non-soliton perturbation will disperse and will also move away from the soliton, because the group velocity for any linear perturbations will be different from the propagation velocity of the soliton.

We wish to find the growth of fluctuations in position $q(\zeta)$. Because the position depends on soliton frequency V, the contributions that arise from both Γ_q and Γ_V must be considered. First,

$$\Gamma_q(\zeta) = \Re\left[\int_{-\infty}^{\infty} d\tau A \tau \operatorname{sech}(A\tau - q) \right.$$

$$\left. \times \exp(-iV\tau - i\theta)\overline{\Gamma}(\tau, \zeta) \right]$$

$$= \int_{-\infty}^{\infty} d\tau A \tau \operatorname{sech}(A\tau - q)$$

$$\times \Re\{\exp(-iV\tau - i\theta)\Gamma\}, \qquad (3.12)$$

$$\Gamma_V(\zeta) = \Re\left[\int_{-\infty}^{\infty} d\tau A(-i)\operatorname{sech}(A\tau - q) \right.$$

$$\left. \times \tanh(A\tau - q)\exp(-iV\tau - i\theta)\overline{\Gamma}(\tau, \zeta) \right]$$

$$= \int_{-\infty}^{\infty} d\tau A \operatorname{sech}(A\tau - q)\tanh(A\tau - q)$$

$$\times \{A \operatorname{sech}(A\tau - q)\Gamma^R$$

$$+ \Im[\exp(-iV\tau - i\theta)\Gamma]\}. \qquad (3.13)$$

From this we can calculate the growth of the fluctuations in velocity:

$$\Delta V(\zeta) = \Delta V(0) + \int_0^{\zeta} d\zeta' \Gamma_V(\zeta')$$

$$= \Re\left[\int_{-\infty}^{\infty} \Delta\phi(\tau, \zeta)\overline{f_V}^* d\tau \right] + \int_0^{\zeta} d\zeta' \Gamma_V(\zeta').$$

$$(3.14)$$

Using the noise correlations calculated above, we can now calculate the correlations in the velocity fluctuations:

$$\langle \Delta V(\zeta)\Delta V^*(\zeta') \rangle$$

$$= \langle \Delta V(0)\Delta V^*(0) \rangle + \int_0^{\zeta}\int_0^{\zeta'} d\zeta'' d\zeta''' \langle \Gamma_V(\zeta'')\Gamma_V^*(\zeta''') \rangle$$

$$= \frac{A}{6\bar{n}} + \left[\frac{\alpha^G A}{3\bar{n}} + \frac{2A^2 \mathcal{I}(t_0)}{\bar{n}} \right]\zeta, \qquad \zeta < \zeta', \quad (3.15)$$

where the overlap integral $\mathcal{I}(t_0)$ is defined as

$$\mathcal{I}(t_0) = \int_{-\infty}^{\infty}\int_{-\infty}^{\infty} d\tau d\tau' \tanh(\tau)\operatorname{sech}^2(\tau)$$

$$\times \tanh(\tau')\operatorname{sech}^2(\tau')\widetilde{\mathcal{F}}(\tau/A - \tau'/A). \quad (3.16)$$

Here $\widetilde{\mathcal{F}}(\tau)$ is the inverse Fourier transform of the fluorescence $\mathcal{F}(\Omega) = 1/2[n_{\text{th}}(\Omega) + 1/2]\alpha^R(\Omega)$.

The correlations in position fluctuations correspond to the jitter in arrival times, because we have chosen a propagative reference frame. The jitter therefore feeds off position fluctuations as well as off noise entering through the velocity:

$$\langle \Delta q(\zeta)\Delta q^*(\zeta') \rangle = \langle (\Delta q(0)\Delta q^*(0))$$

$$+ \int_0^{\zeta}\int_0^{\zeta'} d\zeta'' d\zeta''' [A^2\langle \Delta V(\zeta'')\Delta V^*(\zeta''') \rangle$$

$$+ \langle \Gamma_q(\zeta'')\Gamma_q^*(\zeta''') \rangle], \qquad \zeta < \zeta'.$$

$$(3.17)$$

Thus the timing jitter is

$$\langle [\Delta\tau(\zeta)]^2 \rangle = \langle \Delta q(\zeta)\Delta q^*(\zeta) \rangle$$

$$= \frac{\pi^2}{24\bar{n}} + \frac{\pi^2 \alpha^G}{12\bar{n}}\zeta + \frac{A^3}{6\bar{n}}\zeta^2$$

$$+ \left[\frac{\alpha^G A^3}{9\bar{n}} + \frac{2A^4 \mathcal{I}(t_0)}{3\bar{n}} \right]\zeta^3, \qquad (3.18)$$

which contains cubic terms that are due to the gain and Raman couplings and also slower-growing terms that are due to the initial vacuum fluctuations and amplifier noise.

We note that an alternative method that exploits conserved quantities in the NLS equation is often used[2,14,15] for deriving the timing jitter. The linearized approach that we have presented has the advantage that derivatives of products of stochastic variables do not appear. With such derivatives, the normal rules of calculus do not apply. Rather, the rules of Ito stochastic calculus must be observed, leading to extra drift terms.

B. Dark Solitons

Fibers in the normal dispersion regime can support dark-soliton solutions, so called because they correspond to a dip in the background intensity[16]:

$$\phi_{\text{dark}}(\tau, \zeta) = \phi_0\{1 - A^2 \operatorname{sech}^2[\phi_0 A\tau$$

$$- q(\zeta)]\}^{1/2}\exp[i\theta(\zeta)]\exp[i\sigma(\zeta, \tau)],$$

$$\sigma(\zeta, \tau) = \arcsin\left(\frac{A \tanh[\phi_0 A\tau - q(\zeta)]}{\{1 - A^2 \operatorname{sech}^2[\phi_0 A\tau - q(\zeta)]\}^{1/2}} \right),$$

$$(3.19)$$

where $d\theta/d\zeta = \phi_0^2$, $dq/d\zeta = A\sqrt{1 - A^2}\phi_0^2$, and ϕ_0 is the amplitude of the background field. The size of the intensity dip at the center of the soliton is given by A, with the intensity going to zero in a black $\tanh(\tau)$ soliton, for which $A = 1$. Dark solitons are classed as topological solitons, because they connect two background pulses of different phases. The total phase difference between the boundaries is $\psi = 2 \arcsin(A)$.

The nonvanishing boundary conditions of the dark pulse complicate the perturbation calculation of jitter variance. To ensure that all relevant integrals take on finite values, we impose periodic boundary conditions at $\tau = \pm \tau_l$, which are taken to infinity at the end of the calculation. This situation is equivalent to choosing antiperiodic boundary conditions in a comoving frame, whose velocity is then taken to zero. It requires a soliton solution of the form

$$\phi_{\text{dark}}(\tau, \zeta) = \phi_0 \exp[i\theta(\zeta) - i\kappa\tau]\left\{ \cos\frac{\psi}{2} \right.$$

$$\left. + i\sin\frac{\psi}{2}\tanh\left[\phi_0\tau\sin\frac{\psi}{2} - q(\zeta) \right] \right\},$$

$$(3.20)$$

with a wave number offset $\kappa = (1/\tau_l)$ arctan$\{\tan(\psi/2)\tanh[\phi_0\tau_l\sin(\psi/2)]\}$. The perturbation theory now proceeds in a similar fashion to the bright-soliton case, except that we can greatly simplify the calculation if the unperturbed solution is taken to be a black soliton, i.e., $\psi = \pi$.

The projection functions for the soliton parameters $P_i \in \{\psi, q, \phi_0, \theta\}$ are

$$f_\theta = -\phi_0\tanh(\phi_0\tau - q)\exp(i\theta - i\kappa\tau),$$

$$f_{\phi_0} = i[\tanh(\phi_0\tau - q) + \phi_0\tau\,\text{sech}^2(\phi_0\tau - q)]$$

$$\times \exp(i\theta - i\kappa\tau),$$

$$f_q = -i\phi_0\,\text{sech}^2(\phi_0\tau - q)\exp(i\theta - i\kappa\tau),$$

$$f_\psi = \phi_0[\beta_1\phi_0\tau\tanh(\phi_0\tau - q) - (1/2)]\exp(i\theta - i\kappa\tau),$$

$$(3.21)$$

where $\beta_1 = 1/[2\phi_0\tau_l\tanh(\phi_0\tau_l)]$. For the required adjoint functions we choose

$$\overline{f_q} = \frac{-i3\gamma_q}{4}\,\text{sech}^2(\phi_0\tau - q)\exp(i\theta - i\kappa\tau),$$

$$\overline{f_\psi} = \frac{\gamma_\psi}{\beta_1 - 1}\,\text{sech}^2(\phi_0\tau - q)\exp(i\theta - i\kappa\tau), \quad (3.22)$$

where $\gamma_q = 4/(3\int_{-\phi_0\tau_l}^{\phi_0\tau_l}dt\,\text{sech}^4 t)$ and $\gamma_\psi = (\beta_1 - 1)/\int_{-\phi_0\tau_l}^{\phi_0\tau_l}dt(\beta_1 t\tanh t\,\text{sech}^2 t - \text{sech}^2 t/2)$. The orthogonality condition is now

$$\Re\left(\int_{-\tau_l+q/\phi_0}^{\tau_l+q/\phi_0}d\tau f_{P_i}\overline{f_{P_j}}^* \right) = \delta_{i,j}. \quad (3.23)$$

Once again, we can use the adjoint functions in the linearized equation [Eq. (3.4)] to determine how the fluctuations in position evolve:

$$\frac{\partial}{\partial\zeta}\Delta q(\zeta) = \frac{\phi_0\beta_2}{2}\Delta\psi(\zeta) + \Gamma_q(\zeta),$$

$$\frac{\partial}{\partial\zeta}\Delta\psi(\zeta) = \Gamma_\psi(\zeta), \quad (3.24)$$

where $\beta_2 = \phi_0\tanh(\phi_0\tau_l) - 1/\tau_l$. Here we see how fluctuations in phase produce fluctuations in position. The stochastic term in the equation for ψ evaluates to

$$\Gamma_\psi(\zeta) = \Re\left[\int_{-\tau_l+q/\phi_0}^{\tau_l+q/\phi_0}d\tau\overline{f_\psi}^*(\zeta)\bar\Gamma(\tau, \zeta) \right]$$

$$= \int_{-\tau_l+q/\phi_0}^{\tau_l+q/\phi_0}d\tau\frac{\gamma_\psi}{\beta_1 - 1}\,\text{sech}^2(\phi_0\tau - q)$$

$$\times \{\Re[\exp(-i\phi + i\kappa\tau)\Gamma]$$

$$- \phi_0\tanh(\phi_0\tau - q)\Gamma^R\}, \quad (3.25)$$

from which the correlations of the phase fluctuations can be calculated:

$$\langle\Delta\psi(\zeta)\Delta\psi^*(\zeta')\rangle$$

$$= \langle\Delta\psi(0)\Delta\psi^*(0)\rangle + \int_0^\zeta\int_0^{\zeta'}d\zeta''d\zeta'''\langle\Gamma_\psi(\zeta'')\Gamma_\psi^*(\zeta''')\rangle$$

$$= \frac{\gamma\psi^2}{3\bar n\,\gamma_q\phi_0} + \left[\frac{2\alpha^G\gamma_\psi^2}{3\bar n\,\gamma_q(\beta_1 - 1)^2\phi_0} + \frac{2\gamma_\psi^2\mathcal{I}_{\tau_l}(t_0)}{\bar n(\beta_1 - 1)^2} \right]\zeta,$$

$$\zeta < \zeta', \quad (3.26)$$

where the overlap integral $\mathcal{I}_{\tau_l}(t_0)$ is now defined as

$$\mathcal{I}_{\tau_l}(t_0) = \int_{-\phi_0\tau_l}^{\phi_0\tau_l}\int_{-\phi_0\tau_l}^{\phi_0\tau_l}d\tau d\tau'\tanh(\tau)\text{sech}^2(\tau)\tanh(\tau')$$

$$\times \text{sech}^2(\tau')\widetilde{\mathcal{F}}(\tau/\phi_0 - \tau'/\phi_0). \quad (3.27)$$

The leading order terms for the fluctuations in position are thus

$$\langle\Delta q(\zeta)\Delta q^*(\zeta)\rangle$$

$$= \frac{\phi_0^2\beta_2^2}{4}\int_0^\zeta\int_0^{\zeta'}d\zeta''d\zeta'''\langle\Delta\psi(\zeta'')\Delta\psi^*(\zeta''')\rangle$$

$$= \frac{\phi_0\beta_2^2\gamma_\psi^2}{12\bar n\,\gamma_q}z^2 + \left[\frac{\alpha^G\phi_0\beta_2^2\gamma_\psi^2}{18\bar n\,\gamma_q(\beta_1 - 1)^2} \right.$$

$$\left. + \frac{\mathcal{I}_{\tau_l}(t_0)\phi_0^2\beta_2^2\gamma_\psi^2}{6\bar n} \right]\zeta^3. \quad (3.28)$$

By taking the limit $\tau_l \to \infty$, we find the leading order terms in the jitter growth for a black soliton:

$$\langle[\Delta\tau(\zeta)]^2\rangle = \frac{\phi_0^3}{12\bar n}\zeta^2 + \left[\frac{\alpha^G\phi_0^3}{18\bar n} + \frac{\mathcal{I}(t_0)\phi_0^4}{6\bar n} \right]\zeta^3, \quad (3.29)$$

where the overlap integral $\mathcal{I}(t_0)$ is as defined in Eq. (3.16). As in the anomalous dispersion regime, the vacuum fluctuations contribute to quadratic growth in the jitter variance, and gain and Raman fluctuations contribute to cubic growth. However, the size of the jitter is smaller than that in the bright-soliton case for the same propagation distance ζ. The contribution from the vacuum and gain terms is one half, and the contribution from the Raman term is one quarter, of that in Eq. (3.18), giving dark solitons some advantage over their bright cousins.

4. SCALING PROPERTIES

In summary, there are three different sources of noise in the soliton, all of which must be taken into account for small pulse widths. These noise sources contribute to fluctuations in the velocity parameter, which lead to quadratic or cubic growth in the timing-jitter variance for single-pulse propagation. The noise sources also produce other effects, such as those that are effected through soliton interactions, but we do not consider these here.

Each of the noise sources has different characteristic scaling properties, which are summarized as follows:

A. Vacuum Fluctuations

The vacuum fluctuations cause diffusion in position, which is important for small propagation distances. There are position fluctuations even at the initial position, as the shot noise in the arrival time of individual coherent-state photons gives an initial fluctuation effect. After propagation has started, this initial position fluctuation is increased by the additional variance in the soliton velocity, essentially as a result of randomness in the frequency domain.

For bright solitons the resultant soliton timing variance is given by[10]

$$\langle [\Delta \tau(\zeta)]^2 \rangle_I = \frac{\pi^2}{24\bar{n}} + \frac{1}{6\bar{n}} \zeta^2 \quad \text{(bright)}. \qquad (4.1)$$

For purposes of comparison, note that $\bar{N} = 2\bar{n}$ is the mean photon number for a $\text{sech}(\tau)$ soliton. Numerical calculations confirm that, for $\tanh(\tau)$ dark solitons, the variance was approximately one half of the bright-soliton value, as predicted by the analysis outlined in Subsection 3.B:

$$\langle [\Delta \tau(\zeta)]^2 \rangle_I = \frac{\pi^2}{48\bar{n}} + \frac{1}{12\bar{n}} \zeta^2 \quad \text{(dark)}. \qquad (4.2)$$

This shot-noise effect, which occurs without amplification, is due simply to the initial quantum-mechanical uncertainty in the position and momentum of the soliton. Because of the Heisenberg uncertainty principle, the soliton momentum and position cannot be specified exactly. This effect dominates the Gordon-Haus effect over propagation distances less than a gain length. However, for short pulses, this distance can still correspond to many dispersion lengths, thus generating large position jitter. We note that there are also initial fluctuations in the background continuum, which may feed into the soliton parameters as the soliton propagates. This lesser effect is included in the numerical calculation; a comparison of the numerical results with the analytic results confirms that the initial fluctuations in the soliton parameters account for almost all the shot-noise contribution to the jitter.

B. Gordon–Haus Noise

As is well known, the noise that is due to gain and loss in the fiber produces the Gordon–Haus effect, which is currently considered the major limiting factor in any long-distance soliton-based communications system that uses relatively long ($>$10-ps) pulses. Amplification with mean intensity gain α^G, chosen to compensate for fiber loss, produces a diffusion (or jitter) in position. Unless other measures are taken, for sufficiently small amplifier spacing[4] and at large distances this jitter is given by[2,14,17]

$$\langle [\Delta \tau(\zeta)]^2 \rangle_{GH} \simeq \frac{\alpha^G}{9\bar{n}} \zeta^3 \quad \text{(bright)},$$

$$\langle [\Delta \tau(\zeta)]^2 \rangle_{GH} \simeq \frac{\alpha^G}{18\bar{n}} \zeta^3 \quad \text{(dark)}, \qquad (4.3)$$

in which the linearly growing terms have been neglected.

Another effect of the amplifier noise is to introduce an extra noise term by means of the fluctuations in the Raman-induced soliton self-frequency shift. This term scales as the fifth power of distance and hence will become important for long propagation distances. This combined effect of spontaneous emission noise and the Raman intrapulse scattering has been dealt with by others.[5] The full phase-space equation [Eq. (2.1)] models this effect accurately, as it includes the delayed Raman nonlinearity, and the effect would be seen in numerical simulations carried out over long propagation distances.

C. Raman Noise

A lesser-known effect is the fluctuations in velocity that arise from the Raman phase-noise term Γ^R in Eq. (2.2). Like the Gordon–Haus effect, this Raman noise generates a cubic growth in jitter variance:

$$\langle [\Delta \tau(\zeta)]^2 \rangle_R = \frac{2\mathcal{I}(t_0)}{3\bar{n}} \zeta^3 \quad \text{(bright)},$$

$$\langle [\Delta \tau(\zeta)]^2 \rangle_R = \frac{\mathcal{I}(t_0)}{6\bar{n}} \zeta^3 \quad \text{(dark)}, \qquad (4.4)$$

where $\mathcal{I}(t_0)$ is the integral defined in Eq. (3.16) that indicates the spectral overlap between the pulse spectrum and the Raman fluorescence. The mean-square Raman-induced timing jitter has a cubic growth in both cases, but the dark-soliton variance is one quarter of that of the bright soliton.

The magnitude of this Raman jitter can be found by evaluation of $\mathcal{I}(t_0)$ numerically or else by use of an analytic approximation. An accurate model of the Raman gain, on which $\mathcal{I}(t_0)$ depends, requires a multi-Lorentzian fit to the experimentally measured spectrum.[18] A fit with 11 Lorentzians was used in the numerical simulations, including 10 Lorentzians to model the measured gain and fluorescence accurately. One extra Lorentzian was used at low frequencies to model guided-wave acoustic Brillouin scattering; this has a relatively small effect on an isolated soliton, except to cause phase noise.

For analytic work, however, a single-Lorentzian model[19] can suffice for approximate calculations. A plot of the Raman gain profile $\alpha^R(\Omega)$ for both models is given in QNI, along with a table of the fitting parameters for the multi-Lorentzian model. The spectral features of the Raman noise correlations are determined directly from the Raman fluorescence function $\mathcal{F}(\Omega)$, which we plot in Fig. 1. For the single-Lorentzian model, the fluorescence spectrum is approximately flat at low frequencies:
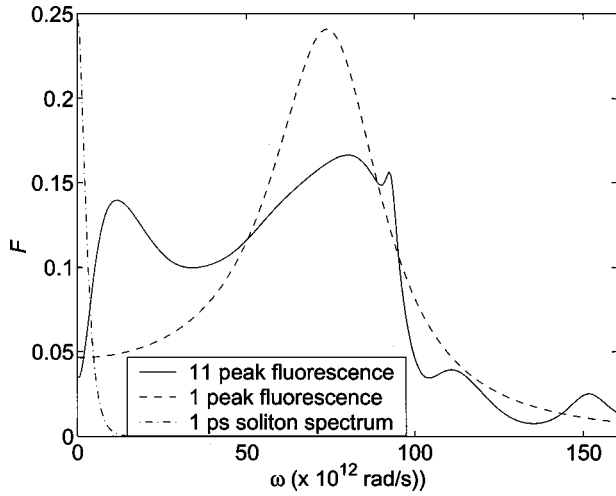
Fig. 1. Spectrum of the fluorescence function $\mathcal{F}(\omega)$ for the 11-Lorentzian model (solid curve) and the single-Lorentzian model (dashed curve) for a temperature of $T = 300$ K.   Also shown is the spectrum of a $t_0 = 1$ ps soliton.

$$\mathcal{F}(\Omega) = \frac{1}{2}\left[n_{\text{th}}(\Omega) + \frac{1}{2}\right]\alpha^R(\Omega)$$

$$\simeq \frac{2F_1\Omega_1\delta_1{}^2 k_B T}{(\Omega_1{}^2 + \delta_1{}^2)^2\hbar} = \mathcal{F}(0), \qquad (4.5)$$

which greatly simplifies the Raman correlations. As Fig. 1 indicates, the spectral overlap of $\mathcal{F}(\Omega)$ with a $t_0 = 1$ ps soliton occurs in this low-frequency region. Thus the white-noise approximation for the Raman correlations is good for solitons of this pulse width and larger. For smaller pulse widths, not only is the Raman contribution to the noise larger because of the greater overlap but the colored nature of the correlations must be taken into account.

In the single-Lorentzian model, $\mathcal{I}(t_0 \to \infty) \simeq (4/15)\mathcal{F}(0)$, which gives

$$\langle[\Delta t(x)]^2\rangle_R \simeq \frac{8|k''|^2 n_2\hbar\omega_0{}^2\mathcal{F}(0)}{45\mathcal{A}ct_0{}^3}x^3$$

$$= \frac{8t_0{}^2\mathcal{F}(0)}{45\bar{n}}\left(\frac{x}{x_0}\right)^3 \quad \text{(bright)},$$

$$\langle[\Delta t(x)]^2\rangle_R \simeq \frac{2|k''|^2 n_2\hbar\omega_0{}^2\mathcal{F}(0)}{45\mathcal{A}ct_0{}^3}x^3$$

$$= \frac{2t_0{}^2\mathcal{F}(0)}{45\bar{n}}\left(\frac{x}{x_0}\right)^3 \quad \text{(dark)}. \qquad (4.6)$$

At a temperature of 300 K, $\mathcal{F}(0) = 4.6 \times 10^{-2}$ when a single Lorentzian centered at 12 THz with fitting parameters $F_1 = 0.7263$, $\delta_1 = 20 \times 10^{12}\, t_0$, and $\Omega_1 = 75.4 \times 10^{12}\, t_0$ is used.

5. NUMERICAL RESULTS

More-precise results can be obtained by numerical integration of the original Wigner phase-space equation, Eq. (2.1), which includes the full time-delayed nonlinear Raman response function. The results for $t_0 = 500$ fs

bright and dark solitons are shown in Figs. 2(a) and 2(b), respectively. The gain and photon number were chosen to be $G = \alpha^G/x_0 = 4.6 \times 10^{-5}\,\text{m}^{-1}$ (0.2 dB/km) and $\bar{n} = 4 \times 10^6$, with $x_0 = 440$ m. These values are based on $\mathcal{A} = 40\,(\mu\text{m})^2$, $k'' = 0.57\,(\text{ps})^2/\text{km}$, and $n_2 = 2.6 \times 10^{-20}\,(\text{m})^2/\text{W}$ for a dispersion-shifted fiber.[20] These numerical calculations use the multiple-Lorentzian model of the Raman response function shown in Fig. 1, which accurately represents the detailed experimental response function.

The numerical method is based on the split-step idea[21] as adapted to Raman propagation.[22] Noise is treated with a central-difference technique that is appropriate to stochastic equations,[23] with the necessary adaptations required for treating a partial stochastic differential equation.[24] We duplicated all calculations, using two different space steps but with the same underlying noise sources, to calculate discretization error. Sampling error was also estimated from the standard central-limit theorem procedure over a large ensemble of noise sources. Tests on time steps and window sizes were also carried out to ensure that there were no errors from these sources.
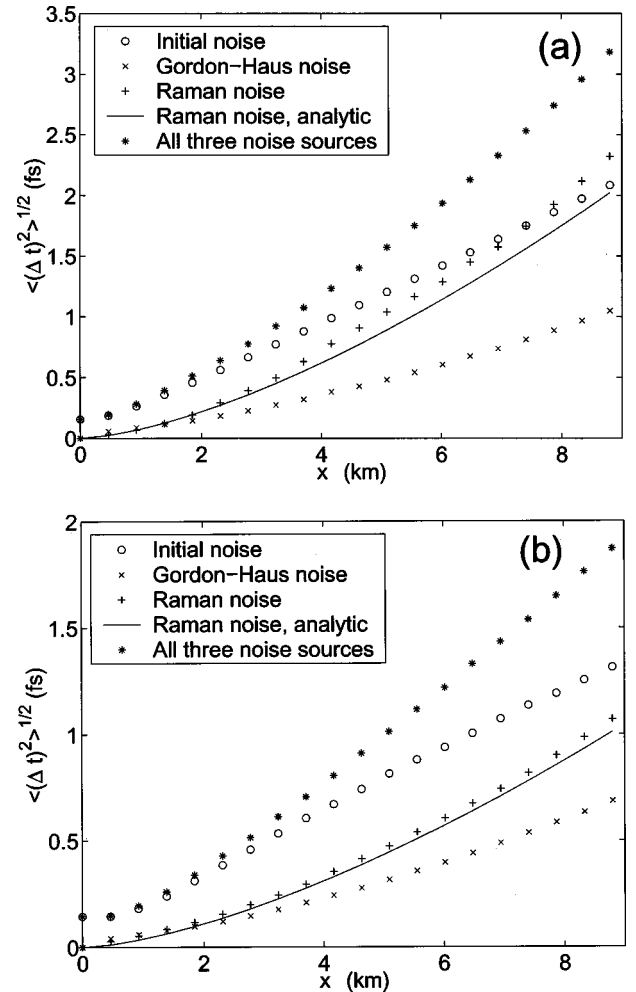
Fig. 2. Timing jitter in $t_0 = 500$ fs (a) bright and (b) dark solitons that is due to initial quantum fluctuations, the Gordon-Haus effect, and Raman noise. The asterisks give the total jitter, and the continuous curve gives the approximate analytic results for the Raman jitter.

The initial conditions consist of a coherent laser pulse injected into the fiber. In the Wigner representation, this minimum uncertainty state leads to the initial vacuum fluctuations. The numerical calculation thereby includes the full effect of these zero-point fluctuations, including the noise that appears in the background continuum and in the soliton parameters. We take the initial pulse shape in the anomalous dispersion regime to be a fundamental bright soliton, with $A = 1$ and $V = \theta = q = 0$. Such a soliton can be experimentally realized with a sufficiently intense pulse, which will be reshaped into a soliton or a soliton train. The nonsoliton part of the wave will disperse, and any extra solitons will move away at different velocities from the fundamental soliton. The numerical simulation in the normal dispersion regime used two black solitons of opposite phase chirp ($A = \pm 1$), so the field amplitude at either boundary was the same. This phase matching ensured the stability of the numerical algorithm, which assumes periodic boundary conditions.

We calculated the position jitter at a given propagation time by combining the waveform with a phase-matched local-oscillator pulse that had a linear chirp in amplitude, and integrating the result to give the soliton position. This homodyne measurement involves symmetrically ordered products, so the Wigner representation will give the correct statistics. The variance in soliton position was then calculated from a sample of 1000 trajectories. For this small distance of propagation ($\simeq 10$ km), the jitter variance that is due to the initial noise is twice the Gordon–Haus jitter, but, for larger distances, the cubic effects are expected to dominate.

For ultrafast pulses, the Raman jitter dominates the Gordon–Haus jitter (by a factor of 2 in the 500-fs bright-soliton case) and will continue to do so even for long propagation distances. For short propagation distances the Gordon–Haus effect is not exactly cubic, because of neglected terms in the perturbation expansion, which give a linear (as opposed to cubic) growth in the jitter variance. However, there are no such terms in the Raman case. The analytic Raman results are also shown in the figures and indicate that our approximate formula gives a reasonable fit to the numerical data even for subpicosecond pulses. With this approximate formula, the relative size of the two effects scales as

$$\frac{\langle [\Delta t(x)]^2 \rangle_R}{\langle [\Delta t(x)]^2 \rangle_{\mathrm{GH}}} = \frac{6 \mathcal{I}(t_0)|k''|}{G t_0{}^2} = \frac{6 \mathcal{I}(t_0)}{G x_0} \simeq \frac{8 \mathcal{F}(0)}{5 G x_0} \quad \text{(bright)},$$

$$\frac{\langle [\Delta t(x)]^2 \rangle_R}{\langle [\Delta t(x)]^2 \rangle_{\mathrm{GH}}} = \frac{3 \mathcal{I}(t_0)|k''|}{G t_0{}^2} = \frac{3 \mathcal{I}(t_0)}{G x_0} \simeq \frac{4 \mathcal{F}(0)}{5 G x_0} \quad \text{(dark)}. \tag{5.1}$$

Expressions (5.1) show why experiments to date,[20] which have used longer pulses ($t_0 > 1$ ps) and dispersion-shifted fiber, have not detected the Raman-noise contribution to the jitter. The Raman jitter exceeds the Gordon–Haus jitter for bright solitons with periods $x_0 < 1.5$ km. Dark solitons, however, have an enhanced resistance to the Raman noise, which means that a shorter period is needed before the Raman jitter will become important.

The total jitter, which corresponds to the realistic case in which all three noise sources are active, is also shown in Fig. 2 and in the bright-soliton case is approximately a factor of 3 larger than the ordinary Gordon–Haus effect, over the propagation distance shown. The physical origin of these quantum-noise sources cannot easily be suppressed. The initial vacuum-induced timing jitter is caused by the shot-noise variance in the soliton guiding frequency. The physical origin of the Raman jitter is in frequency shifts that are due to soliton phase modulation by the ever-present quantum and thermal phonon fields in the fiber medium.

The numerical method should give accurate results far beyond the distance shown in Fig. 2, provided that the transverse and propagative resolutions are made large enough. The equations generated in the Wigner method should remain valid up to $\zeta \sim \sqrt{\bar{n}}$, which corresponds to ~ 1000 km. When the Wigner equations can no longer be trusted, the positive-P equations will still give accurate results. In this paper we have not analyzed any multi-soliton effects, although the numerical method does simulate interactions between solitons. This analysis just requires that the initial conditions and the simulation window width be set up according to whether interactions are to be considered. We have not included third-order dispersion in our model; it would become important for very small pulses ($t_0 \simeq 100$ fs) but could easily be included in the equations for numerical simulation.

The approximate analytic results are most limited probably by their exclusion of Raman intrapulse effects, such as the deterministic self-frequency shift and the amplifier jitter that feeds through this. Approximate calculations[5] of the self-frequency shift jitter variance show that it grows as the fifth power of distance. With our parameters and the measured value of the Raman time constant,[6] it would become larger than the usual Gordon–Haus effect at $x \simeq 100$ km, or ~ 10 times the propagation distance shown in Fig. 2. Using standard techniques,[5] one could extend the perturbation theory presented in this paper to include the self-frequency shift contributions (from both the amplifier noise and Raman phase noise) to the total jitter.

6. CONCLUSIONS

Our major conclusion is that quantum-noise effects that are due to the intrinsic finite-temperature phonon reservoirs are a dominant source of fluctuations in phase and arrival time for subpicosecond solitons. For longer solitons, Raman effects are reduced compared with the Gordon–Haus jitter from the laser gain medium that is needed to compensate for losses. The reason for this is the smaller intensity of the pulse and therefore the reduced Raman couplings that occur for longer solitons, which are less intense than shorter solitons with the same dispersion. The ratio can be calculated simply from the product $G x_0$, which gives the gain per soliton length. A smaller x_0 corresponds to a shorter, more intense soliton and hence to a larger Raman noise, whereas a larger G corresponds to increased laser gain with larger spontaneous noise.

At a given pulse duration and fiber length, a strategy for testing this prediction would be to use short pulses with dispersion-shifted fiber that has an increased dispersion, because this increases the relative size of the Raman jitter. The physical reason for this effect is simple. Solitons have an intensity that increases with dispersion if everything else is unchanged. At the same time, the multiplicative phase noise found in Raman propagation is proportional to intensity and hence becomes relatively large compared with the additive Gordon–Haus noise that is due to amplification. For large enough dispersion, the temperature-dependent Raman jitter should become readily observable at short enough distances that amplification is unnecessary. This temperature dependence would give a completely unambiguous signature of the effect that we have calculated. A mode-locked fiber soliton laser would be a suitable pulse source, owing to the very short (64-fs), quiet pulses[25,26] that are obtainable.

ACKNOWLEDGMENTS

REFERENCES

1. J. F. Corney, P. D. Drummond, and A. Liebman, "Quantum noise limits to terabaud communications," Opt. Commun. **140**, 211–215 (1997).
2. J. P. Gordon and H. A. Haus, "Random walk of coherently amplified solitons in optical fiber transmission," Opt. Lett. **11**, 665–667 (1986).
3. P. D. Drummond and J. F. Corney, "Quantum noise in optical fibers. I. Stochastic equations," J. Opt. Soc. Am. B **18**, 139–152 (2001).
4. L. F. Mollenauer, J. P. Gordon, and M. N. Islam, "Soliton propagation in long fibers with periodically compensated loss," IEEE J. Quantum Electron. **22**, 157–173 (1986).
5. J. D. Moores, W. S. Wong, and H. A. Haus, "Stability and timing maintenance in soliton transmission and storage rings," Opt. Commun. **113**, 153–175 (1994).
6. A. K. Atieh, P. Myslinski, J. Chrostowski, and P. Galko, "Measuring the Raman time constant (T_R) for soliton pulses in standard single-mode fiber," J. Lightwave Technol. **17**, 216–221 (1999).
7. D.-M. Baboiu, D. Mihalache, and N.-C. Panoiu, "Combined influence of amplifier noise and intrapulse Raman scattering on the bit-rate limit of optical fiber communication systems," Opt. Lett. **20**, 1865–1867 (1995); D. Mihalache, L.-C. Crasovan, N.-C. Panoiu, F. Moldoveanu, and D.-M. Baboiu, "Timing jitter of femtosecond solitons in monomode optical fibers," Opt. Eng. **35**, 1611–1615 (1996); D. Wood, "Constraints on the bit rates in direct detection optical communication systems using linear or soliton pulses," J. Lightwave Technol. **8**, 1097–1106 (1990).
8. D. Shenoy and A. Puri, "Compensation for the soliton self-frequency shift and the third-order dispersion using bandwidth-limited optical gain," Opt. Commun. **113**, 410–406 (1995); S. V. Chernikov and S. M. J. Kelly, "Stability of femtosecond solitons in optical fibres influenced by optical attenuation and bandwidth limited gain," Electron. Lett. **28**, 238–240 (1992).
9. G. P. Agrawal, *Nonlinear Fiber Optics*, 2nd ed. (Academic, San Diego, Calif. 1995), p. 475.
10. P. D. Drummond and W. Man, "Quantum noise in reversible soliton logic," Opt. Commun. **105**, 99–103 (1994).
11. H. A. Haus and W. S. Wong, "Solitons in optical communications," Rev. Mod. Phys. **68**, 423–444 (1996).
12. F. X. Kartner, D. J. Dougherty, H. A. Haus, and E. P. Ippen, "Raman noise and soliton squeezing," J. Opt. Soc. Am. B **11**, 1267–1276 (1994).
13. D. J. Kaup, "Perturbation theory for solitons in optical fibers," Phys. Rev. A **42**, 5689–5694 (1990).
14. Y. S. Kivshar, M. Haelterman, P. Emplit, and J. P. Hamaide, "Gordon–Haus effect on dark solitons," Opt. Lett. **19**, 19–21 (1994); Y. S. Kivshar, "Dark solitons in nonlinear optics," IEEE J. Quantum Electron. **29**, 250–264 (1993).
15. I. M. Uzunov and V. S. Gerdjikov, "Self-frequency shift of dark solitons in optical fibers," Phys. Rev. A **47**, 1582–1585 (1993).
16. A. Hasegawa and F. Tappert, "Transmission of stationary nonlinear optical pulses in dispersive dielectric fibers. II. Normal dispersion," Appl. Phys. **23**, 171–172 (1973).
17. J. Hamaide, P. Emplit, and M. Haelterman, "Dark-soliton jitter in amplified optical transmission systems," Opt. Lett. **16**, 1578–1580 (1991).
18. R. H. Stolen, C. Lee, and R. K. Jain, "Development of the stimulated Raman spectrum in single-mode silica fibers," J. Opt. Soc. Am. B **1**, 652–657 (1984); D. J. Dougherty, F. X. Kartner, H. A. Haus, and E. P. Ippen, "Measurement of the Raman gain spectrum of optical fibers," Opt. Lett. **20**, 31–33 (1995); R. H. Stolen, J. P. Gordon, W. J. Tomlinson, and H. A. Haus, "Raman response function of silica-core fibers," J. Opt. Soc. Am. B **6**, 1159–1166 (1989).
19. Y. Lai and S.-S. Yu, "General quantum theory of nonlinear optical-pulse propagation," Phys. Rev. A **51**, 817–829 (1995); S.-S. Yu and Y. Lai, "Impacts of self-Raman effect and third-order dispersion on pulse squeezed state generation using optical fibers," J. Opt. Soc. Am. B **12**, 2340–2346 (1995).
20. A. Mecozzi, M. Midrio, and M. Romagnoli, "Timing jitter in soliton transmission with sliding filters," Opt. Lett. **21**, 402–404 (1996); L. F. Mollenauer, P. V. Mamyshev, and M. J. Neubelt, "Measurement of timing jitter in filter-guided soliton transmission at 10 Gbits/s and achievement of 375 Gbits/s-Mm, error free, at 12.5 and 15 Gbits/s," Opt. Lett. **19**, 704–706 (1994); L. F. Mollenauer, M. J. Neubelt, S. G. Evangelides, J. P. Gordon, J. R. Simpson, and L. G. Cohen, "Experimental study of soliton transmission over more than 10000 km in dispersion-shifted fiber," Opt. Lett. **15**, 1203–1205 (1990).
21. P. D. Drummond, "Central partial difference propagation algorithms," Comput. Phys. Commun. **29**, 211–225 (1983).
22. P. D. Drummond and A. D. Hardman, "Simulation of quantum effects in Raman-active waveguides," Europhys. Lett. **21**, 279–284 (1993).
23. P. D. Drummond and I. K. Mortimer, "Computer simulations of multiplicative stochastic differential equations," J. Comput. Phys. **93**, 144–170 (1991).
24. M. J. Werner and P. D. Drummond, "Robust algorithms for solving stochastic partial differential equations," J. Comput. Phys. **132**, 312–326 (1997).
25. C. X. Yu, S. Namiki, and H. A. Haus, "Noise of the stretched pulse fiber laser. II. Experiments," IEEE J. Quantum Electron. **33**, 660–668 (1997).
26. S. Namiki, C. X. Yu, and H. A. Haus, "Observation of nearly quantum-limited timing jitter in an all-fiber ring laser," J. Opt. Soc. Am. B **13**, 2817–2823 (1996).